THE JOURNAL OF PHYSICAL CHEMISTRY Letters

Letter

pubs.acs.org/JPCL

Velocity Distribution of Hydrogen Atom Spin Polarization

Bernadette M. Broderick,[†] Yumin Lee,[†] Michael B. Doyle,[†] Oleg S. Vasyutinskii,[‡] and Arthur G. Suits*,[†]

[†]Department of Chemistry, Wayne State University, Detroit Michigan 48202, United States

[‡]Ioffe Institute, Russian Academy of Sciences, St. Petersburg 19401, Russia

ABSTRACT: We present an experimental technique allowing for direct measurement of the velocity dependence of hydrogen atom spin polarization with high resolution and high sensitivity. The strategy is a simple adaptation of the H atom Rydberg time-of-flight approach, here demonstrated for 213 nm photodissociation of HBr. The two coherent contributions to the spin polarization are measured for H atoms produced in conjunction with dissociation to Br($^2P_{3/2}$) and Br*($^2P_{1/2}$); they are found to be negligible for the former channel but substantial for the latter, in qualitative agreement with values inferred from previous theoretical predictions of the Br atom polarization. The ratio of the measured spin polarization anisotropy parameters directly gives the asymptotic scattering phase shift for dissociation along the two potentials for the H + Br* channel. The approach is general and suitable for application to polyatomic molecules or to scattering studies.

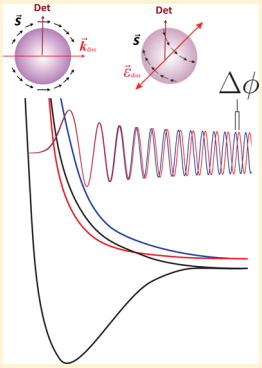

SECTION: Spectroscopy, Photochemistry, and Excited States

Investigations of orbital polarization in photodissociation or scattering have become a powerful means of probing details of atomic and molecular interactions,[1,2] revealing nonadiabatic dynamics,[3] matter−wave interference effects,[4] new conservation laws,[5] and other new phenomena.[6] As hydrogen atoms are a primary photoproduct for countless important molecules, there is a strong motivation to extend these studies to H atoms, for which spin is the only form of angular momentum. In this case, the H atom spin can be used as a reporter on orbital orientation, nonadiabatic dynamics, and coherent dissociation mechanisms underlying these processes.[3] The production of spin-polarized hydrogen atoms (SPHs) in photodissociation of hydrogen halides was predicted over 30 years ago,[7,8] but experimental schemes to quantify this have proved elusive. The reason for this is that laser probes cannot directly interrogate spin; therefore, magnetic fields are needed to break the degeneracy, allowing laser-based spin selectivity. A convenient means to achieve this is to use the orbital motion imparted to the electron during detection to create the necessary magnetic field. This spin−orbit interaction splits the degeneracy, allowing for a frequency-dependent probe that is spin-selective and well-defined in the laboratory frame. However, the greatest spin−orbit splitting in the hydrogen atom occurs at the 2p level, and it is only 0.36 cm^{-1}, generally far smaller than the associated Doppler width of any dissociation or scattering event of interest.

In recent studies, the angular distribution of H atom photofragment spin polarization has been inferred from measurements of the angular momentum polarization of the Cl or Br cofragment in photodissociation of HCl and HBr.[9−12] Rakiktzis and co-workers have also reported one scheme for probing of H atom spin polarization in photodissociation;[13] however, the resolution and sensitivity were inadequate to characterize the underlying photochemical processes, and the results could only be shown to be consistent with inferences based upon other measurements. In this Letter, we outline a simple modification of the widely used H atom Rydberg time-of-flight technique to allow direct probing of the velocity dependence of the H atom spin polarization with the very high velocity resolution and excellent sensitivity that this technique offers.[14] Our first application of this spin-polarized hydrogen Rydberg time-of flight (SPH-RTOF) method is a study of photodissociation of HBr at 212.8 nm, where previous theoretical calculations are available.[15]

Photofragment H atom spin polarization is an example of rank-one photofragment orientation.[16] This orientation may be characterized by three anisotropy parameters given in the laboratory frame description of Vasyutinskii and co-workers[17] as γ_1, γ_1', and α_1. The first, γ_1, reflects a coherent dissociation process involving parallel and perpendicular components induced by circularly polarized photolysis light. The second, γ_1', also reflects coherent dissociation involving both parallel and perpendicular components but induced by linearly polarized photolysis light. The third, α_1, arises from incoherent dissociation via perpendicular transitions induced by circularly polarized photolysis light.[18] These parameters characterize the magnitude of the molecular-frame spin components s_y, s_x, and s_z, respectively.[18] Each of these contibutions has distinct angular distributions with characteristic sensitivity in specific probe geometries, and this is what allows for a simple decomposition of their contributions using the approach described here. All of these may be probed using circularly polarized light, and by

Received: September 15, 2013
Accepted: October 1, 2013
Published: October 1, 2013

   dx.doi.org/10.1021/jz401982a | *J. Phys. Chem. Lett.* 2013, 4, 3489−3493

taking difference signals of the right circularly polarized (RCP) and left circularly polarized (LCP) probe (or equivalently by varying the photolysis polarization), one may isolate the corresponding orientation signal from the population signals. In the work described here, we probe the two coherent contributions as this may be achieved in a convenient geometry without scanning the probe lasers. We also sketch our future plans for measuring α_1.

Our experimental geometries are summarized in Figure 1. The dissociation laser intersects a molecular beam of HBr at

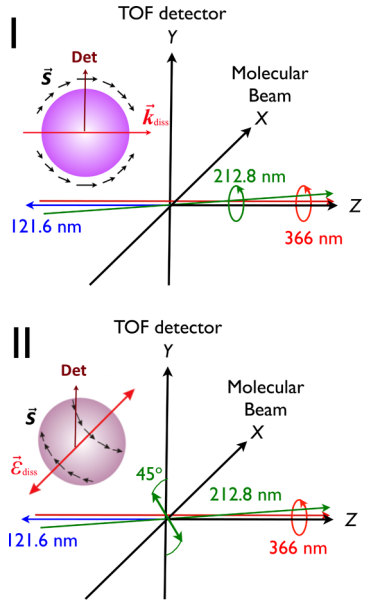

Figure 1. Experimental geometries employed. The photolysis laser (212.8 nm), Lyman-α (121.6 nm), and tagging laser (366 nm) all propagate parallel to the laboratory Z axis. The inset in each is a schematic view of the angular distribution of the associated spin polarization detected in each geometry. For geometry II, the inset cartoon is shown with the Z axis into the figure.

right angles, nearly parallel to the two laser beams involved in the double-resonant excitation to a high-n Rydberg state. The photolysis (212.8 nm) and "tagging" lasers (366 nm) copropagate counter to the Lyman-α beam. Neutral H atoms fly 28 cm perpendicular to the laser and molecular beam where they are field-ionized (detector acceptance 2°) and counted as a function of time after the dissociation. Three aspects of the experiment are necessary for this approach to work: (1) the spin polarization angular distributions for the three parameters are disjoint, that is, specific recoil directions in particular probe geometries are sensitive only to one parameter at a time, (2) the double-resonance detection scheme described below is spin-sensitive if a single fine structure component can be isolated, and (3) the Rydberg time-of-flight approach can readily achieve Doppler selectivity of 3% for the fastest fragments, which is more than enough to ensure the needed fine structure selectivity if either of the two excitation lasers are narrow enough in line width to achieve this as well. The Rydberg tagging approach nicely satisfies these conditions. The angular distribution of the spin polarizations for γ_1 and γ_1' are also shown schematically in Figure 1. For circularly polarized photolysis light, the coherent spin polarization is maximal for recoil perpendicular to the laser propagation direction, while the incoherent (α_1) spin polarization vanishes along that direction. The single measurement of the spin polarization along that direction thus cleanly and completely characterizes the velocity-dependent coherent spin polarization arising from circularly polarized photolysis light. For dissociation by linearly polarized photolysis, the spin polarization is maximal for recoil 45° to the light polarization. Measurement of the spin polarization along that direction completely characterizes γ_1', which is the only possible spin polarization resulting from linearly polarized photolysis radiation.

The spin-sensitive detection scheme is summarized in Figure 2 for a RCP tagging beam. With the tagging laser **k** vector

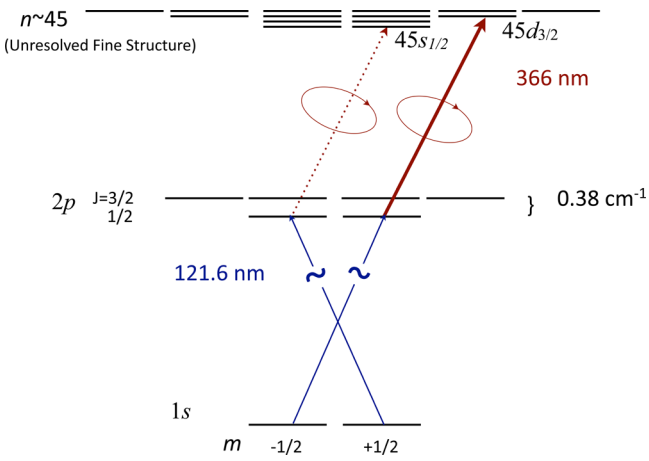

Figure 2. Spin-sensitive double resonance excitation scheme.

defining the quantization axis, the linearly polarized Lyman-α laser excites the two H atom 1s magnetic sublevels to the 2p level. The laser is tuned to the line center for the $2p_{1/2}$ level. Spin selectivity comes in the tagging step, which is illustrated in the figure for RCP probe light and n = 45, but the spin sensitivity is similar for any high-n Rydberg that is well isolated from nearby levels. There are two possible excitation pathways, $1s_{1/2} \rightarrow 2p_{1/2} \rightarrow 45s_{1/2}$ or $45d_{3/2}$. However, the radial integrals for transitions to the $45s_{1/2}$ Rydberg state are about 37 times smaller than those to the $45d_{3/2}$; therefore, we neglect that contribution. This leads to a very simple result. The absorption intensity I is given by

$$I_r = C[1 - \langle s_Z \rangle] \quad (1)$$

where $\langle s_Z \rangle$ is an average value of the spin component along the direction of the tagging beam propagation (laboratory Z axis).

The absorption intensity I_r in eq 1 is given for the Lyman-α light polarization perpendicular to Z and the 366 nm tagging beam RCP propagating along +Z. If it is LCP, the sign in the second term in eq 1 is replaced by (+). C is a constant that depends on the beam intensities and the reduced transition matrix elements. The sensitivity of the experimental signal to the initial state spin polarization is given by

$$\frac{I_r - I_l}{I_r + I_l} = -\langle s_Z \rangle = -\frac{1}{2}\frac{(N_{1/2} - N_{-1/2})}{(N_{1/2} + N_{-1/2})} \quad (2)$$

where $N_{1/2}$ and $N_{-1/2}$ are the H atom m-state populations. In the experiment, we may vary either the tagging laser polarization or the photolysis to obtain these difference signals. In practice, we find that varying the photolysis polarization results in more stable signals, although for clarity, we write these expressions for modulation of the probe polarization.

dx.doi.org/10.1021/jz401982a | J. Phys. Chem. Lett. 2013, 4, 3489−3493

The experimental H atom time-of-flight results for HBr photolysis at 212.8 nm are shown in Figure 3 for geometries I and II. Two peaks are seen in each spectrum, corresponding to coincident formation of $Br(^2P_{3/2})$ and $Br^*(^2P_{1/2})$ in the photodissociation process. A velocity resolution of 0.5% full width at half-maximum is easily obtained. As the photolysis polarization is changed (from RCP to LCP in geometry I or +45 to −45° in geometry II), little difference is seen in the H atom signal at shorter times that is produced in conjunction with Br, while that formed in conjunction with Br* shows a significant modulation in both geometries. Integration of the peaks for 16 scans of 2 min each gives the results compiled in Table 1. In separate experiments with linearly polarized probe and photolysis light, we obtained values for the anisotropy parameter β, which characterizes the overall photoproduct angular distribution via $I(\theta) \propto 1 + \beta(P_2(\cos\theta))$, with P_2 as the second Legendre polynomial, and the branching fraction $\Gamma = \sigma(Br^*)/(\sigma(Br) + \sigma(Br^*))$. These are also shown in Table 1 and compared to previous work.

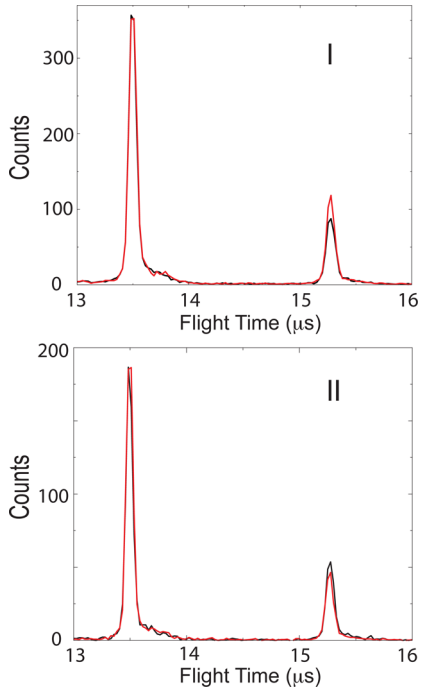

Figure 3. H atom time-of-flight spectra for 212.8 nm photolysis of HBr for the indicated experimental geometry. The red curve corresponds to the RCP probe, and the black curve corresponds to the LCP probe.

For the H + Br* channel in geometry I, we find $\langle s_Z\rangle = -0.18$, implying a net spin orientation counter to the propagation direction of the RCP photolysis laser. In geometry II, with the photlysis polarization at +45°, we obtain $\langle s_Z\rangle = 0.19$, implying spin polarization along the Z axis. The result for the spin sensitivity given in eq 2 can readily be recast in terms of the anisotropy parameters using expressions given in ref 18. This yields, for geometry I

$$\frac{I_r - I_l}{I_r + I_l} = -\langle s_Z\rangle = -\frac{3\sqrt{3}\gamma_1}{4\left(1 - \frac{\beta}{4}\right)} \quad (3)$$

and for geometry II

$$\frac{I_r - I_l}{I_r + I_l} = -\langle s_Z\rangle = -\frac{3\sqrt{3}\gamma_1'}{4\left(1 + \frac{\beta}{4}\right)} \quad (4)$$

Table 1. Summary of Experimental Results for Anisotropy Parameters and Br* Branching Fraction[a]

	H + Br	H + Br*
	−0.97(2)	**0.95(10)**
β	-1^b	1^b
	-1^c	0^c
	-1^d	1.27^d
Γ		**0.19(2)**
		$0.17(2)^b$
		0.14^c
		0.18^d
γ_1(H)	**0.00(4)**	**−0.10(4)**
γ_1(Br,Br*)	0.005^c	-0.31^c
γ_1'(H)	**0.03(2)**	**0.18(9)**
γ_1'(Br,Br*)	-0.001^c	0.24^c
$\Delta\phi(a^3\Pi_{0+},t^3\Sigma_1)$ (H)		**2.08(0.34)**
$\Delta\phi(a^3\Pi_{0+},t^3\Sigma_1)$ (Br*)		2.23^c

[a]The present results are in bold. The uncertainties in the parentheses are 2σ based on 10 measurements. The phase shift is in radians. [b]Reference 19. [c]Reference 15. [d]Reference 20. The β parameter is inferred from Σ/Π branching.

Using these expressions and the data shown in Figure 3, we obtain the anisotropy parameters γ_1 and γ_1', and these are reproduced in Table 1 after accounting for hyperfine depolarization, which reduces the experimental signals by 1/2 on a time scale of 0.7 ns.[9] These may be compared to the molecular frame anisotropy parameters[21] after converting the latter using the expressions given in refs 22 and 23. For the H + Br channel, the H spin polarization is zero within the uncertainty for both coherent parameters, as expected for a dissociation that is almost exclusively perpendicular in character. For the Br* channel, a significant effect is seen, and we find that the values for γ_1 and γ_1' are similar in magnitude and opposite in sign.

Before discussing the interpretation of these results, we briefly summarize the ultraviolet photochemistry of HBr. The dominant contributions are perpendicular transitions from the $X^1\Sigma^+$ ground state to $A^1\Pi_1$ and $a^3\Pi_1$ excited states, adiabatically correlating with $H(^2S_{1/2}) + Br(^2P_{3/2})$, and parallel transitions to $a^3\Pi_{0+}$ and perpendicular transitions to $t^3\Sigma_1$, adiabatically correlating with $H(^2S_{1/2}) + Br(^2P_{1/2})$.[15,19] Near-limiting perpendicular anisotropy is seen in dissociation for the Br channel, but for the Br* channel, the anisotropy parameter β is found to be strongly wavelength-dependent.[13,19,24,25] The Br* branching fraction Γ also shows an interesting wavelength dependence, consistently 15% except in the region around 235 nm where it rises to 25%. Rakitzis and co-workers reported a slice-imaging study of the angular momentum polarization of both Br and Br* at 193 nm.[10,26] They obtained the molecular-frame orientation parameters for Br and Br* produced at 193 nm by circularly polarized photolysis light, corresponding to the lab-frame α_1 and γ_1 discussed here for hydrogen atoms. Raktizis and co-workers subsequently reported the only direct measure of the H atom spin polarization in photodissociation.[13] This study of HBr and HCl at 193 nm was obtained via Doppler scanning of circularly polarized Lyman-α under bulb conditions with detection of polarized fluorescence to isolate a single fine structure component in the excitation step. The

dx.doi.org/10.1021/jz401982a | J. Phys. Chem. Lett. 2013, 4, 3489−3493

approach did not resolve the H atom recoil speed and thus could not disentangle the underlying Br and Br* contributions. However, the results were found to be consistent with the earlier halogen atom measurements.

Using high-level ab initio methods, Smolin et al. determined potential energy curves, transition moments, and nonadiabatic couplings for all relevant electronic states and performed wavepacket dynamics on these curves.[15] The curves relevant to the H + Br* channel are schematically reproduced in Figure 4.

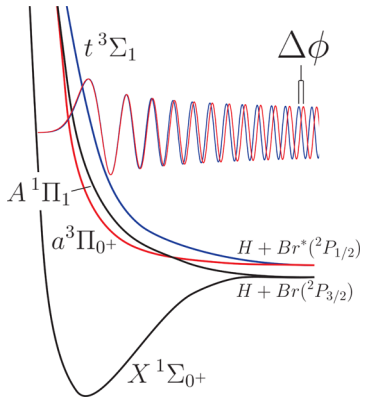

Figure 4. Potential energy curves for HBr relevant to the H + Br* channel. The scattering phase shift $\Delta\phi$ derived from the measured H atom spin polarization is shown schematically arising from interference between dissociation along the $a^3\Pi_{0+}$ and $t^3\Sigma_1$ curves.

They obtained all possible anisotropy parameters for the Br and Br* products and identified the two states responsible for the changing Br* angular distributions, the parallel $a^3\Pi_{0+}$ state at long wavelength and perpendicular dissociation via $t^3\Sigma_1$ at shorter wavelengths populated via nonadiabatic transitions from the $^{1,3}\Pi_1$ states. It is interference between dissociation along these two paths that gives rise to the spin polarization observed here. More recently, Valero et al. used HBr photodissociation as a test case to examine the possibility of using a spin-coupled diabatic representation to construct potential curves for semiclassical trajectory studies.[20] Their results reproduced many of the features of the Smolin et al. study, but they found a somewhat larger $X^1\Sigma_{0+} \rightarrow a^3\Pi_{0+}$ transition dipole moment.

Our experimental results allow for a direct comparison of the H atom spin polarization at 213 nm to the theoretical predictions given by Smolin et al.[15] for the Br and Br* cofragment polarization after converting the latter to the laboratory frame.[22,23] This comparison is especially easy to do for the H + Br* channel because the anisotropy parameters for H and Br* determined should be identical as they are both $J = 1/2$ systems.[18] The polarization parameters given by Smolin et al.[15] for Br* are given together with our data for H in Table 1. For both Br* parameters, the values are nearly equal and opposite in sign, just as seen in our results for the SPH parameters. However, they are significantly larger. This may be a consequence of the fact that the parallel contribution is too low in the calculations,[15] so that the parallel and perpendicular contributions are nearly equal, giving near-maximal values for these coherent parameters. This is suggested both by the fact that the β parameter values calculated in ref 15 were significantly lower than experimental ones and that upon obtaining a larger parallel contribution, Valero et al.[20] obtained the cusp seen in the experimental branching to Br* and a β value closer to experiment. Our experimental values of the H polarization parameters in the H + Br channel can also be compared with the theoretical values for $Br(^2P_{3/2})$,[15] which are given in the second column in Table 1. However, in this case, the H and Br polarization parameters are not constrained to be identical, and additional polarization data on Br are needed for comparison.[13] Some of these data are not presently available, but as both the experimental and theoretical values of the polarization parameters are very small, such a detailed analysis is not warranted.

We can also obtain the asymptotic scattering phase shifts for dissociation to H + Br* along the $a^3\Pi_{0+}$ and $t^3\Sigma_1$ curves directly from the ratio of these parameters[27]

$$\Delta\phi(a^3\Pi_{0+}, t^3\Sigma_1) = \tan^{-1}\left(\frac{\gamma_1'}{\gamma_1}\right) \quad (5)$$

The results obtained are also given in Table 1 and compared to the theoretical results from Smolin et al., where a good agreement is seen. The meaning of this phase shift is shown schematically in Figure 4. Coherent dissociation along the $a^3\Pi_{0+}$ and $t^3\Sigma_1$ potentials gives rise to matter−wave interference that results in H atom spin polarization. This phase shift is a sensitive probe of the differences in the potentials and the excitation energy.[4]

The present results show the capability for SPH-RTOF to yield fundamental insights into molecular scattering processes. Applications to dissociation of polyatomic molecules and reactive and inelastic scattering promise new detail concerning these elementary processes. Analogous coherent effects are anticipated in dissociation of polyatomic molecules.[28] We note that we have not measured the incoherent α_1 parameter in this study; it would require a different geometry and scanning of the probe laser. However, we have found that this same double-resonance excitation scheme may be used with prompt field ionization in an ion imaging approach so that all three parameters could be determined in a single experimental configuration. This effort is currently underway.

AUTHOR INFORMATION

Corresponding Author

*E-mail: asuits@wayne.edu.

Notes

The authors declare no competing financial interest.

ACKNOWLEDGMENTS

This work was supported by the National Science Foundation under Award Number 1111348. We thank Jingong Zhang, Floyd Davis, Vladimir Chernyak, and Frederic Merkt for helpful discussions.

REFERENCES

(1) Suits, A. G.; Vasyutinskii, O. S. Imaging Atomic Orbital Polarization in Photodissociation. *Chem. Rev.* **2008**, *108*, 3706−3746.

(2) Clark, A.; Brouard, M.; Quadrini, F.; Vallance, C. Atomic Polarization in the Photodissociation of Diatomic Molecules. *Phys. Chem. Chem. Phys.* **2006**, *8*, 5591−5610.

(3) Bracker, A.; Wouters, E.; Suits, A.; Vasyutinskii, O. Imaging the Alignment Angular Distribution: State Symmetries, Coherence Effects and Nonadiabatic Interactions in Photodissociation. *J. Chem. Phys.* **1999**, *110*, 6749−6765.

(4) Rakitzis, T.; Kandel, S.; Alexander, A.; Kim, Z.; Zare, R. Photofragment Helicity Caused by Matter−Wave Interference from Multiple Dissociative States. *Science* **1998**, *281*, 1346−1350.
(5) Krasilnikov, M. B.; Kuznetsov, V. V.; Suits, A. G.; Vasyutinskii, O. S. Vector Correlations in Photodissociation of Polarized Polyatomic Molecules Beyond the Axial Recoil Limit. *Phys. Chem. Chem. Phys.* **2011**, *13*, 8163−8174.
(6) Herath, T.; Yan, L.; Lee, S. K.; Li, W. Strong-Field Ionization Rate Depends on the Sign of the Magnetic Quantum Number. *Phys. Rev. Lett.* **2012**, *109*, 1079−7114.
(7) Vasyutinskii, O. Orientation of Atoms during Photodissociation of Molecules. *Sov. Phys. JETP Lett.* **1980**, *31*, 428.
(8) Vasyutinskii, O. Contribution to the Theory of the Effect of Orientation of Atoms Produced in Photodissociation of Molecules. *Sov. Phys. JETP* **1981**, *54*, 855−861.
(9) Rakitzis, T. P.; Samartzis, P. C.; Toomes, R. L.; Kitsopoulos, T. N.; Brown, A.; Balint-Kurti, G. G.; Vasyutinskii, O. S.; Beswick, J. A. Spin-Polarized Hydrogen Atoms from Molecular Photodissociation. *Science* **2003**, *300*, 1936.
(10) Rakitzis, T. P.; Samartzis, P. C.; Toomes, R. L.; Kitsopoulos, T. N. Measurement of Br Photofragment Orientation and Alignment from HBr Photodissociation: Production of Highly Spin-Polarized Hydrogen Atoms. *J. Chem. Phys.* **2004**, *121*, 7222.
(11) Rakitzis, T. P. Pulsed-Laser Production and Detection of Spin-Polarized Hydrogen Atoms. *ChemPhysChem* **2004**, *5*, 14.
(12) Rakitzis, T. P. Highly Spin-Polarized Atoms and Molecules from Rotationally State-Selected Molecules. *Phys. Rev. Lett.* **2005**, *94*, 083005.
(13) Sofikitis, D.; Rubio-Lago, L.; Bougas, L.; Alexander, A. J.; Rakitzis, T. P. Laser Detection of Spin-Polarized Hydrogen from HCl and HBr Photodissociation: Comparison of H- and Halogen-Atom Polarizations. *J. Chem. Phys.* **2008**, *129*, 144302.
(14) Krautwald, H. J.; Schnieder, L.; Welge, K. H.; Ashfold, M. N. Hydrogen-Atom Photofragment Spectroscopy. Photodissociation Dynamics of H_2O in the B−X Absorption Band. *Faraday Discuss. Chem. Soc.* **1986**, *82*, 99−110.
(15) Smolin, A. G.; Vasyutinskii, O. S.; Balint-Kurti, G. G.; Brown, A. Photodissociation of HBr. 1. Electronic Structure, Photodissociation Dynamics, and Vector Correlation Coefficients. *J. Phys. Chem. A* **2006**, *110*, 5371−5378.
(16) Siebbeles, L.; Glass-Maujean, M.; Vasyutinskii, O.; Beswick, J.; Roncero, O. Vector Properties in Photodissociation: Quantum Treatment of the Correlation Between the Spatial Anisotropy and the Angular Momentum Polarization of the Fragments. *J. Chem. Phys.* **1994**, *100*, 3610.
(17) Picheyev, B.; Smolin, A.; Vasyutinskii, O. Ground State Polarized Photofragments Study by Using Resonance and Off-Resonance Probe Beam Techniques. *J. Phys. Chem. A* **1997**, *101*, 7614−7626.
(18) Wouters, E. R.; Ahmed, M.; Peterska, D. S.; Bracker, A. S.; Suits, A. G.; Vasyutinskii, O. S. In *Imaging in Chemical Dynamics*; Suits, A. G., Continetti, R. E., Eds.; American Chemical Society: Washington, DC, 2000.
(19) Regan, P. M.; Langford, S. R.; Orr-Ewing, A. J.; Ashfold, M. N. The Ultraviolet Photodissociation Dynamics of Hydrogen Bromide. *J. Chem. Phys.* **1999**, *110*, 281.
(20) Valero, R.; Truhlar, D. G.; Jasper, A. W. Adiabatic States Derived from a Spin-Coupled Diabatic Transformation: Semiclassical Trajectory Study of Photodissociation of HBr and the Construction of Potential Curves for $LiBr^+$. *J. Phys. Chem. A* **2008**, *112*, 5756−5769.
(21) Rakitzis, T.; Zare, R. Photofragment Angular Momentum Distributions in the Molecular Frame: Determination and Interpretation. *J. Chem. Phys.* **1999**, *110*, 3341.
(22) Alexander, A. J. Determination of the Helicity of Oriented Photofragments. *J. Chem. Phys.* **2005**, *123*, 194312.
(23) Costen, M. L.; Hall, G. E. Coherent and Incoherent Orientation and Alignment of ICN Photoproducts. *Phys. Chem. Chem. Phys.* **2007**, *9*, 272−287.
(24) Magnotta, F.; Nesbitt, D. J.; Leone, S. R. Excimer Laser Photolysis Studies of Translational-to-Vibrational Energy Transfer. *Chem. Phys. Lett.* **1981**, *83*, 21−25.
(25) Xu, Z.; Koplitz, B.; Wittig, C. Kinetic and Internal Energy Distributions via Velocity-Aligned Doppler Spectroscopy: The 193 nm Photodissociation of H_2S and HBr. *J. Chem. Phys.* **1987**, *87*, 1062.
(26) Rakitzis, T.; Samartzis, P.; Toomes, R.; Tsigaridas, L.; Coriou, M.; Chestakov, D.; Eppink, A.; Parker, D.; Kitsopoulos, T. Photofragment Alignment from the Photodissociation of HCl and HBr. *Chem. Phys. Lett.* **2002**, *364*, 115.
(27) Balint-Kurti, G. G.; Orr-Ewing, A.; Beswick, J.; Brown, A.; Vasyutinskii, O. Vector Correlations and Alignment Parameters in the Photodissociation of HF and DF. *J. Chem. Phys.* **2002**, *116*, 10760.
(28) Lee, S. K.; Townsend, D.; Vasyutinskii, O. S.; Suits, A. G. $O(^1D_2)$ Orbital Orientation in the Ultraviolet Photodissociation of Ozone. *Phys. Chem. Chem. Phys.* **2005**, *7*, 1650−1656.